Arabinoxylan in Water through SANS: Single-Chain Conformation, Chain Overlap, and Clustering

Maike Petermann, Lucie Dianteill, Amal Zeidi, Roméo Vaha Ouloassekpa, Paul Budisavljevic, Claude Le Men, Cédric Y Montanier, Pierre Roblin, Bernard Cabane, Ralf Schweins, et al.

Arabinoxylan in Water Through SANS: Single Chain Conformation, Chain Overlap and Clustering

Maike Petermann,[†,1] *Lucie Dianteill,*[†,1] *Amal Zeidi,*[†] *Roméo Vaha Ouloassekpa,*[†] *Paul Budisavljevic,*[†] *Claude Le Men,*[†] *Cédric Montanier,*[†] *Pierre Roblin,*[‡] *Bernard Cabane,*[#] *Ralf Schweins,*[‖] *Claire Dumon,*[†] *Antoine Bouchoux*[*,†]

[†]TBI, Université de Toulouse, CNRS, INRAE, INSA, Toulouse, France

[‡]Laboratoire de Génie Chimique, Université de Toulouse, CNRS, INPT, UPS, Toulouse, France

[#]LCMD, CBI, ESPCI - Paris Tech, 75231 Paris, France

[‖]Institut Laue-Langevin, DS/LSS, 71 Avenue des Martyrs, CS-20156, 38042 Grenoble, France

[1]Both authors contributed equally to the work

ABSTRACT

Using small-angle neutron scattering (SANS), we examine the structure and conformational behavior of wheat arabinoxylan (AX) prepared at various concentrations in a sodium phosphate aqueous buffer. As for another major hemicellulose, xyloglucan, we observe a small number of large clusters, surrounded by AX chains that behave exactly as a polymer in good solvent with a

Flory exponent $\nu = 0.588$. The fit of the data at high q-values to a standard worm-like chain model gives the persistence length $l_p = 45$ Å, and cross-section of the chains, $2R_c = 11\text{-}12$ Å. In addition, using a dedicated modeling approach, we extract from the SANS data at intermediate q-range the correlation length ξ of the solutions in the semidilute regime. The decay of ξ with concentration follows a scaling law that further confirms the self-avoiding statistical behavior of the AX chains. This first comprehensive study about the properties of water-soluble AX at different length scales may certainly help in the development of products and/or processes involving AX as a substitute to fossil carbon molecules.

GRAPHICAL ABSTRACT

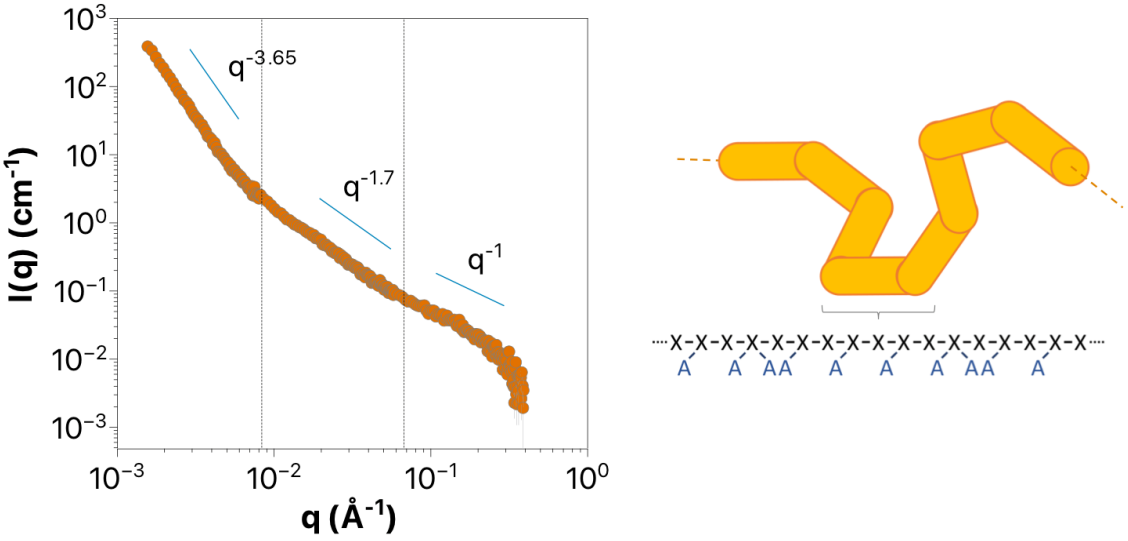

INTRODUCTION

During evolution, plants have gained an outstanding diversity of structures and chemical compositions.[1] De facto, many of the biomolecules found in plant cell walls are interesting

alternatives to fossil carbon molecules for producing fuels, plastics, or other value chemicals.[2] Arabinoxylan (AX), a polysaccharide, is one of these promising biopolymers. AX is the main hemicellulose in grasses such as wheat and rye. It is the second-most abundant polysaccharide - after cellulose- in these species, and it is readily available as by-product of the corresponding agro-industrial processes.[3] AX is a linear chain that consists in a (1,4)-β-D-linked xylose (X) backbone decorated with arabinose (A) substitutions on the second and/or third carbon. Additional occasional substitutions are acetate or glucuronic acid decorations, which are found to be involved in the interaction between AX and cellulose microfibrils *in planta*.[4] Ferulic acid residues can also be found on the arabinose side chain, and in this case are involved in the covalent binding of AX with lignin in the plant cell wall.[5]

Historically, AXs extracted from plant biomass were first used for their viscous nature, improving the property of dough in bread-making for instance.[6] Nowadays, their use as thickeners or emulsifiers becomes increasingly common in the food industry,[7] with recent researches that even suggest a positive health effect of AX addition.[8] Other applications are based on the film-forming properties of AXs,[9] or their ability to form gels through interchain covalent linkage between ferulic acid residues.[10] The natural propensity of AX to interact with cellulose also makes it a natural candidate for coating dedicated surfaces and/or designing composite objects for specific applications.[11–14]

Depending on the plant source and/or extraction process, AXs have diverse chemical compositions with respect to their A/X number ratio, and the presence or not of additional substitutions, i.e. acetate, glucuronic, ferulic. Accordingly, a fair number of research works deals with the chemical characterization of AXs from different sources,[6,15–17] with some attempts to link the chemical composition of the biopolymer to its macroscopic physicochemical properties such

as solubility,[12] or rheology.[18] Here we focus on a simple version of AX extracted from wheat, which is a water-soluble AX that lacks any substitutions other than arabinose residues. One important reason for this choice is that the solubility in water is a crucial parameter with respect to applications, where it is much more practicable to use solutions of a polymer in processes and operations that must be reproducible. As demonstrated by Köhnke et al.,[12] solubility in water is ensured when the A/X number ratio is high, typically > 0.5. At such degree of substitution, the A residues are sufficiently evenly distributed on the chain to prevent associative interactions between unsubstituted X residues (presumably *via* hydrogen-bonds).[19]

Surprisingly, the question of the conformation and organization of AX chains when dispersed in water is still not clear, whereas this information is essential for the applications cited above and for developing new ones. To our knowledge, the most complete dataset is the one provided by Dervilly-Pinel et al. in the early 2000's, where water-soluble AX are characterized using rheology, size exclusion chromatography (SEC) and multi-angle laser light scattering (MALS).[20] However, as pointed out later on by Picout et al.,[21] those results only lead to an indirect and questionable quantification of some polymer parameters, namely the polymer-solvent interactions (Flory exponent ν) and the chain flexibility (persistence length l_p). Interestingly, small-angle scattering techniques (X-rays, SAXS, or neutrons, SANS) are able to directly quantify those values, as it was nicely demonstrated by Muller et al. in their pioneering work on xyloglucan (XG), another hemicellulose.[22]

Here we examine solutions of AX prepared in controlled conditions (pH, ionic strength), using a sodium phosphate aqueous buffer. The first objective of this work consists in accurately determining the properties of a *single chain* of AX in these conditions, as it is done in Muller's study on XG.[22] For that, we focus on SANS data obtained in a q-range that informs about the

conformational statistics at intermediate (coil) scale, down to the persistence length and the equivalent cross-section of the chain. We discuss the results in light of the chemical structure of the AX source, and in comparison with recent SANS results on non-soluble AX polymers.[18]

Our second objective is to focus on the AX chain behavior at high concentration, namely in the *semidilute regime* where the AX concentration C is higher than the overlap concentration C^*; the latter being determined precisely through viscosity measurement. The main question is how the characteristic length scale of the polymer solution, i.e., the correlation length ξ, evolves with C. This question is clearly of fundamental interest, with still a limited number of experimental works that measure ξ and confront these measurements with theoretical scaling predictions,[23,24] especially for polysaccharides. On the other hand, the general behavior of AX chains in the semidilute regime, and the change in ξ as a function of C, are also crucial information for applications where the concentration of polymer in solution has to be maximized and/or where the diffusional properties of the polymer solution must be controlled.[25]

EXPERIMENTAL SECTION

Material and Sample Preparation. AX, extracted and purified from wheat flour, was purchased from Megazyme (Wicklow, Ireland). The same lot, reference P-WAXYL n°120601, was used for preparing all the samples. The product is a slightly yellowish powder that contains ~95% AX in mass. The AX chains have a A/X molar ratio of 38/62. According to previous HPLC and NMR analyses,[12,26] this arabinoxylan source is free from traces of ferulic or glucuronic acid so that the AX chains are fully neutral. In these works and others, AX solutions of 5 to 10 $g.L^{-1}$ are prepared by vigorously mixing the powder with water at high temperature (40-100 °C) for a given time (from 10 minutes to a few hours).[12,20,26] The AX chains are in all cases considered as

completely dissolved, as in the work of Köhnke et al.[12] for instance, where a 10 g.L^{-1} AX solution prepared in such a way has no measurable turbidity at 700 nm.[12] However, as described in the Supporting Information, we find from SAXS experiments that, even if the solutions indeed appear translucid, aggregates are still present and prevent a proper analysis of the solution structure (Figure S1). These aggregates presumably originate from strong and pre-existing interactions between AX chains in the powder. One way to dissolve such aggregates is to lower the AX concentration to 1 g.L^{-1} during the solubilization at high temperature. For reaching higher AX concentrations, we then extract water from the solution using the osmotic stress technique, as detailed hereafter. In the SAXS and SANS spectra of concentrated AX solutions prepared in that way, the presence of aggregates is greatly reduced, and the signature of individual AX chains is then clearly visible (Figure S1 and Figure 3). Note however that there is still an intensity upturn at low q-values ($< 7 \times 10^{-3}$ Å^{-1}) in all our samples, which suggests that it is not possible to get rid of all associative interactions between the AX chains. We discuss this feature in the text in light of the works of Muller et al.[27] and Yu et al.[18] on XG and AX from *Plantago ovata*, respectively.

Unless noted otherwise, all samples were thus prepared starting from a low-concentration, 1 g.L^{-1}, AX solution. This very solution was itself prepared by mixing for 2 h at 90 °C the AX powder in a volume of a 50 mM sodium phosphate aqueous buffer at pH 6. We chose to use a buffer rather than MilliQ water to ensure that the physicochemical conditions are the same in all cases. Also, this buffer is the one that we use in a further study that aims at investigating the degradation of AX by enzymes that are active in these buffer conditions (ongoing experiments). As the AX is fully neutral, electrostatic interactions should not have any effect on its conformational properties at the different length scales. This contrasts with charged polymers for which the persistence length l_p (stiffness), for instance, depends on the ionic strength and/or pH of the buffer. However, we cannot

entirely rule out that the presence of sodium phosphate could alter in some extent the effective quality of water as a solvent, thus influencing the chain properties as compared to the pure water case. We are probably not talking about a major effect on the conformation of the chains at the length scales examined in this work. But as we do not have any direct evidence of the absence or presence of such a phenomenon, one must keep in mind that the results and properties reported in this work are for AX chains in a specific pH-buffered aqueous solution of 50 mM sodium phosphate.

After cooling to room temperature, the 1 $g.L^{-1}$ AX solution was simply diluted in buffer for preparing solutions at $C < 1$ $g.L^{-1}$. On the other hand, and as already mentioned, solutions at $C > 1$ $g.L^{-1}$ were prepared by concentrating 1 $g.L^{-1}$ AX solutions using osmotic stress, still at room temperature. Osmotic stress is based on water exchange between the sample and a reservoir of controlled osmotic pressure, generally a polyethylene glycol (PEG) solution.[28,29] Briefly, 1 $g.L^{-1}$ AX solutions were placed in 6000-8000 $g.mol^{-1}$ cutoff dialysis bags (Spectra/Por 1 RC, Spectrum , US) that were immersed in a 100-fold volume of PEG solutions prepared in the same buffer at known concentrations. We used PEG20000 (Sigma-Aldrich, US) at concentrations from 50 to 250 $g.L^{-1}$, which corresponds to osmotic pressures between 2.5 kPa and 1 MPa.[30,31] The difference in osmotic pressure between the sample and the reservoir causes the buffer (water and ions) to flow out of the sample, while the AX and PEG cannot pass through the dialysis membrane. This leads to a slow and gentle concentration (from one day to one week, with regular refills of the bags with fresh AX solution) of the AX samples at different levels as a function of the PEG concentration. Note that our intention was not to actually measure the osmotic pressure of the AX solutions using the osmotic stress technique, which is beyond the scope of this paper as it would require dedicated and even more delicate experiments.[28,31,32] Therefore we did not wait for the thermodynamic

equilibrium between the bags and the PEG solutions. We rather simply followed the concentration process in real-time using refractometry (see next section), until a desired concentration was reached in the bags.

For SANS experiments, one sample was prepared at 0.9 $g.L^{-1}$ AX in a deuterated sodium phosphate buffer at pD 6 using the same protocol, i.e., 90 °C and 2 h. In the case of low concentration and consequently low scattered intensity, we used D_2O instead of H_2O to take advantage of the small incoherent scattering from D_2O.[33]

Polymer concentration. For practical and cost-effective reasons, we prepared only small volumes of sample using the osmotic stress technique. As a result, the AX concentration could not be determined accurately through drying as the remaining mass was generally too small. We therefore used refractometry for measuring the AX concentration in those samples. We used a standalone refractometer (Mettler Toledo RM50, CH) that only requires 500 µL of sample per measurement. The increment in refractive index dn relative to pure buffer was measured at 25 °C and converted into AX concentration using $dn/dC = 0.146$ $mL.g^{-1}$.[20] We double-checked this dn/dC value using the refractometer of the SEC-MALS chain (Size exclusion chromatography coupled to multi-angle light scattering, next section) and standard AX samples prepared at 1-5 $g.L^{-1}$ (Figure S2). We were also able to both measure dn and determine the AX concentration through drying for two concentrated samples for which we had enough volume (25 and 30 $g.L^{-1}$). Again, a dn/dC value 0.146 $mL.g^{-1}$ was found (Figure S2). For higher dn values, we considered that the linear relationship between n and C is conserved, as for simple monosaccharide solutions in a similar range of concentration.[34]

Size exclusion chromatography coupled to multi-angle light scattering (SEC-MALS). The SEC-MALS analysis was performed with a setup composed of three SEC columns connected in

series (Shodex OH-Pak SB-805 HQ, SB-803 HQ, SB-802.5 HQ, Showa Denko, JP), a differential refractometer, and a DAWN HELEOS light scattering detector (Wyatt Technology, US). The mobile phase was 50 mM sodium phosphate buffer in MilliQ water, pH 6, with a flow rate of 0.8 $mL.min^{-1}$. A 1 $g.L^{-1}$ AX sample was prepared in the same buffer and filtered through a 0.22 μm syringe filter (Sartorius, DE). 50 μL of this sample was injected in the system, the elution and detection temperatures being set to 25 °C. The refractive index (RI) and light scattering data (LS) data were analyzed using the ASTRA software (version 7) from Wyatt Technology. A dn/dC of 0.146 $mL.g^{-1}$ was used for the data treatment.

Rheology. The rheology measurements were performed with a HAAKE MARS III (Thermo Scientific, US) using a cone and plate geometry of diameter 60 mm and angle 1°. The viscosity was measured at 25 °C, as a function of shear rate in the range 0.1-100 s^{-1}. All the samples investigated, from 0.2 to 30 $g.L^{-1}$ in AX, behave as Newtonian fluids over this range, leading to one average value of the dynamic viscosity η. The viscosity of pure buffer at 25 °C was measured in the same way and found to be $\eta_0 = 8.74 \times 10^{-4}$ Pa.s. This allowed to calculate the so-called specific viscosity, η_{sp} which gives the additional contribution of the polymer to the solution viscosity as compared to the buffer only

$$\eta_{sp} = \left(\frac{\eta-\eta_0}{\eta_0}\right) \quad (1)$$

For concentrations < 4 $g.L^{-1}$, the reduced and inherent viscosities, η_{red} and η_i were calculated according to

$$\eta_{red} = \left(\frac{\eta-\eta_0}{\eta_0}\right)/C \quad (2)$$

and

$$\eta_i = \ln\left(\frac{\eta}{\eta_0}\right)/C \quad (3)$$

The intrinsic viscosity [η] was determined by plotting either η_{red} or η_i as a function of C (Huggins' and Kraemer's plot, respectively) and extrapolating to zero concentration.[35]

Small-angle Neutron Scattering. The SANS experiments were performed on the D11 instrument, Institut Laue-Langevin (ILL, Grenoble, France) during the experiment numbered 9-13-718 (https://doi.org/10.5291/ILL-DATA.9-13-718). We present the results for samples prepared at four AX concentrations: 0.9 (in D_2O buffer), 14, 56 and 135 $g.L^{-1}$. The 0.9 and 14 $g.L^{-1}$ samples were placed in 5- and 1-mm path length quartz cells (Hellma Analytics, DE), respectively. The 56 and 135 $g.L^{-1}$ were much more viscous and placed in specific sandwich cells of 1 mm path length, closed by two quartz windows (Hellma Analytics, DE). The sample cells were positioned in a rack that was thermostatically controlled at 37 °C. This temperature, which is 12 Kelvin higher than the one used in the SEC-MALS and theology experiments, was chosen both for practical and time-related reasons: the data presented here are part of a larger set of SANS measurements aiming at following the enzymatic degradation of the polymer with an enzyme that work at 37°C. We considered that this small difference in temperature would not significantly impact the conformational properties of the chains, neither the main results of the rheology (C^*) and SEC-MALS (molecular weights) experiments, hence our choice to present the data at those two temperatures. The neutron scattering intensities were collected at neutron wavelength 6 Å and at three sample-to-detector distances: 1.4, 8 and 39 m. The intensities were radially averaged, merged and arranged as a function of scattering vector q in the range $q \approx 1.5\times10^{-3} - 3.9\times10^{-1}$ $Å^{-1}$. The corrections for instrumental background, empty cell, and transmission, as well as the normalization to absolute intensities, were achieved following the standard procedures of D11. The sample background was determined from the intensity signal of pure buffer solutions in H_2O

and D_2O. It was then subtracted from the intensity scattered from the samples to obtain the intensity from the solute only.

RESULTS AND DISCUSSION

In the following, we first present and discuss some general features and properties of the AX chains and AX solutions, as obtained using SEC-MALS and viscosity measurements. In a second section, we give a general description of the SANS profiles obtained at the different AX concentrations. The third section focuses on the single-chain properties of AX as determined by modeling the SANS data at intermediate and high q-values. The final section is dedicated to the behavior of the AX polymer solution at concentrations > C^* and the determination of the correlation length ξ as a function of C.

Size distribution and overlap concentration.

Table 1. SEC-MALS analysis of the arabinoxylan (AX) chains

Sample	M_n[a] (10^3 g.mol^{-1})	M_w[b] (10^3 g.mol^{-1})	M_w/M_n[c]	R_g[d] (Å)
Wheat arabinoxylan Megazyme P-WAXYL lot 120601	73.5 ± 15%	168.9 ± 8%	2.3 ± 16%	633 ± 9%

[a]Number-averaged molecular weight, [b]weight-averaged molecular weight, [c]polydispersity index, [d]R_g is the mass-averaged root mean square radius of the polymer chain. Here we report the z-averaged value calculated from the SEC-MALS data over the elution time, as it is commonly done when using this technique. The mass recovery was 96.3%.

Figure 1 and Table 1 give the results obtained using SEC-MALS with an AX solution of 1 g.L^{-1} prepared using the previously described solubilization protocol. Here, the sample was further filtered through a syringe filter with a 0.22 µm molecular weight cut-off.

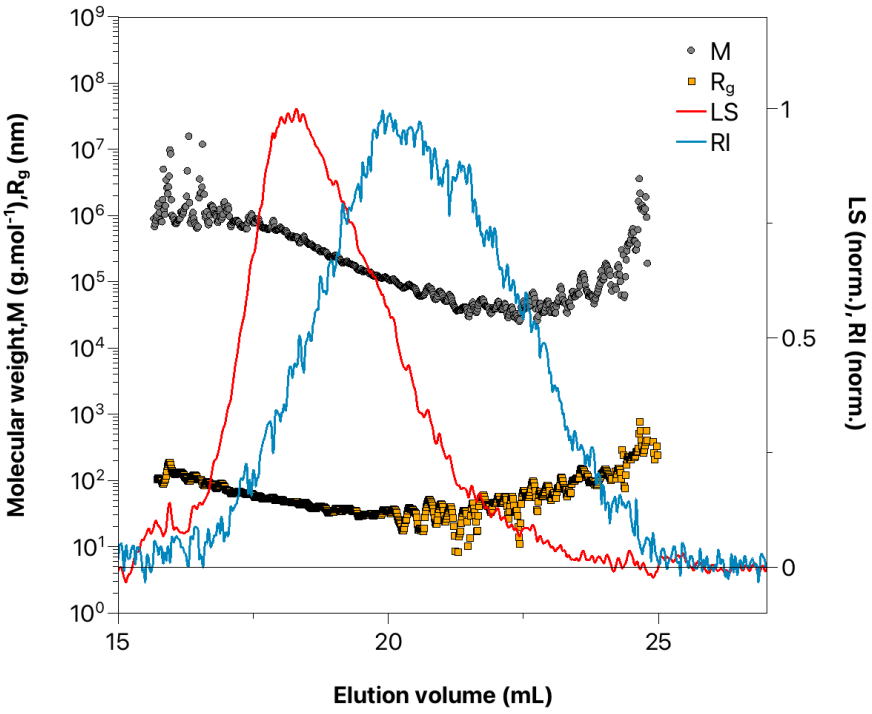

Figure 1. SEC-MALS profile of a 1 g.L^{-1} AX solution. We refer the reader to the Supporting Information (section SEC-MALS analysis, Figure S3) for additional information about the principle of the SEC-MALS technique and the way the average properties of the chains (Table 1) are calculated.

The first important pieces of information are the mass recovery which is > 95%, and the absence of any large objects in the SEC profile (Figure 1). This clearly indicates that the solution is free of the large and strong aggregates observed in SAXS with solutions prepared using less cautious protocols (Figure S1), and confirms that the polymer chains are in a well hydrated state when following our solubilization protocol.[22] However, in SAXS (Figure S1, compressed sample at 8.3 g.L^{-1}) and in the following SANS results (Figure 3), we note that large objects are still visible a

low q-values. Such objects are also observed in XG solutions in pure water,[22,27] and with AX extracted from *Plantago ovata* seed mucilage that form gels in water but that is in a fully hydrated state in 0.7 M KOD solution.[18] As concluded in those previous works, these are most probably weak aggregates or clusters, presumably made from the H-bonded mediated association of a few AX chains. As they form spontaneously, these associative entities cannot be removed from the bulk and are inevitably present in solution. However, they are probably weak enough to be broken by the high shear experienced in the SEC columns, which would explain why they are not detected using SEC-MALS (see the description of Figure S3).[22]

Overall, the data in Table 1 shows that the AX chains are quite polydisperse, with $M_w/M_n >> 1$. Considering the average number of arabinose decorations per xylose, the obtained weight averaged molecular weight M_w corresponds to a chain backbone of ~800 xylose monomers, while the M_n value gives ~350 xylose monomers.

The viscosities of AX solutions at concentrations ranging from 0.2 to 30 g.L^{-1} are given in Figure 2. The inset shows the plots of the reduced (η_{red}, eq 2) and inherent (η_i, eq 3) viscosities which, extrapolated to zero concentration, give an estimation of the intrinsic viscosity [η] of the polymer.[35] Both extrapolations give the same value of [η] ≈ 3 g.dL^{-1}.

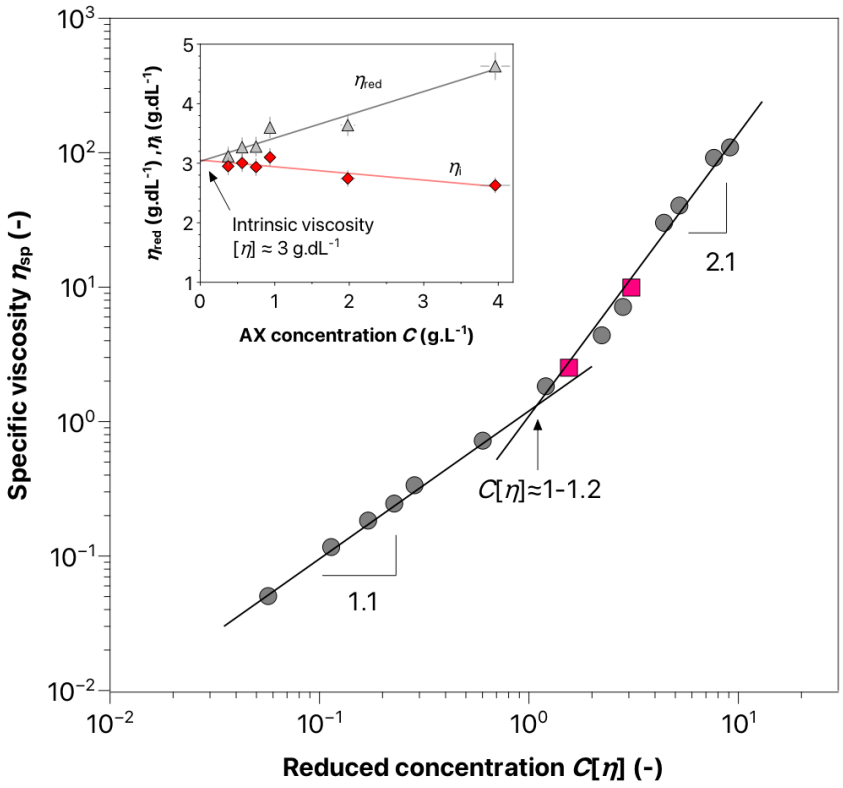

Figure 2. Specific viscosity η_{sp} as a function of AX reduced concentration $C[\eta]$ for AX solutions prepared at low concentration ($C < 1$ g.L^{-1}) and then compressed using the osmotic stress technique (gray circles). We also show results obtained with AX solutions directly prepared at concentration 10 g.L^{-1} and 5 g.L^{-1} at 90 °c for 2 h (purple squares). The inset gives the so-called Huggins' and Kraemer's plots of the reduced (η_{red}) and inherent (η_i) viscosities, respectively, for $C \leq 4$ g.L^{-1}.

Figure 2 displays the variation of the specific viscosity (η_{sp}, eq 1) as a function of $C[\eta]$. On such a log-log representation, the change of slope indicates the crossover from the dilute regime, where the AX chains are independent and do not interact with each other, to the semidilute unentangled regimes where the chains overlap. This crossover takes place at $C[\eta] \approx$ 1-1.2, which is consistent with the theoretical value for linear chains, $C[\eta] = 1$.[27] This gives an overlap AX concentration C^* ≈ 3.3-3.9 g.L^{-1}. Also the slopes of ~1.1 and ~2.1 in the dilute and semidilute regimes, respectively,

are in very good agreement with the values reported for XG (another linear neutral polymer) in good solvent,[27] and also with the values for a linear polyelectrolyte in an excess of salt, which in this case behaves like neutral polymers as electrostatic interactions are entirely screened.[36]

Accordingly, the large clusters that we know are present in the AX solutions do not seem to have any visible impact on the viscosity of the solutions. This is a point that has already been discussed by Muller et al. for XG solutions, where the authors explain that only a few links are possible per XG chain, leading to clusters that have a structure "not far from a linear chain" and thus a viscosity behavior that is similar to a linear chain.[27] An additional explanation would be that the relative number of these clusters is too low for contributing substantially to the viscosity of the solutions. The two square points in Figure 2 are the viscosities measured for AX solutions directly prepared at 5 and 10 $g.L^{-1}$, i.e., without using osmotic compression. In such solutions, we know from our preliminary SAXS results (Figure S1) that AX aggregates are much more present than in solutions prepared through osmotic stress. The fact that the viscosities measured for these two samples fall in line with the other points further suggests that the quantity of AX associative entities is in all cases negligible with regard to the viscosity of the AX solutions.

SANS / General features. We now move on to the SANS characterization of the AX chains, with a first general analysis of the scattering curves obtained at different concentrations (Figure 3). The 0.9 $g.L^{-1}$ solution was prepared in a D_2O buffer solution to maximize the signal-to-background ratio at such a low concentration. The other solutions (14-135 $g.L^{-1}$) were prepared in a H_2O buffer, using the osmotic stress technique. Note the high quality of those SANS data in terms of statistics (small error bars) and q-values that are explored (from 1.5×10^{-3} $Å^{-1}$ to 3.9×10^{-1} $Å^{-1}$).

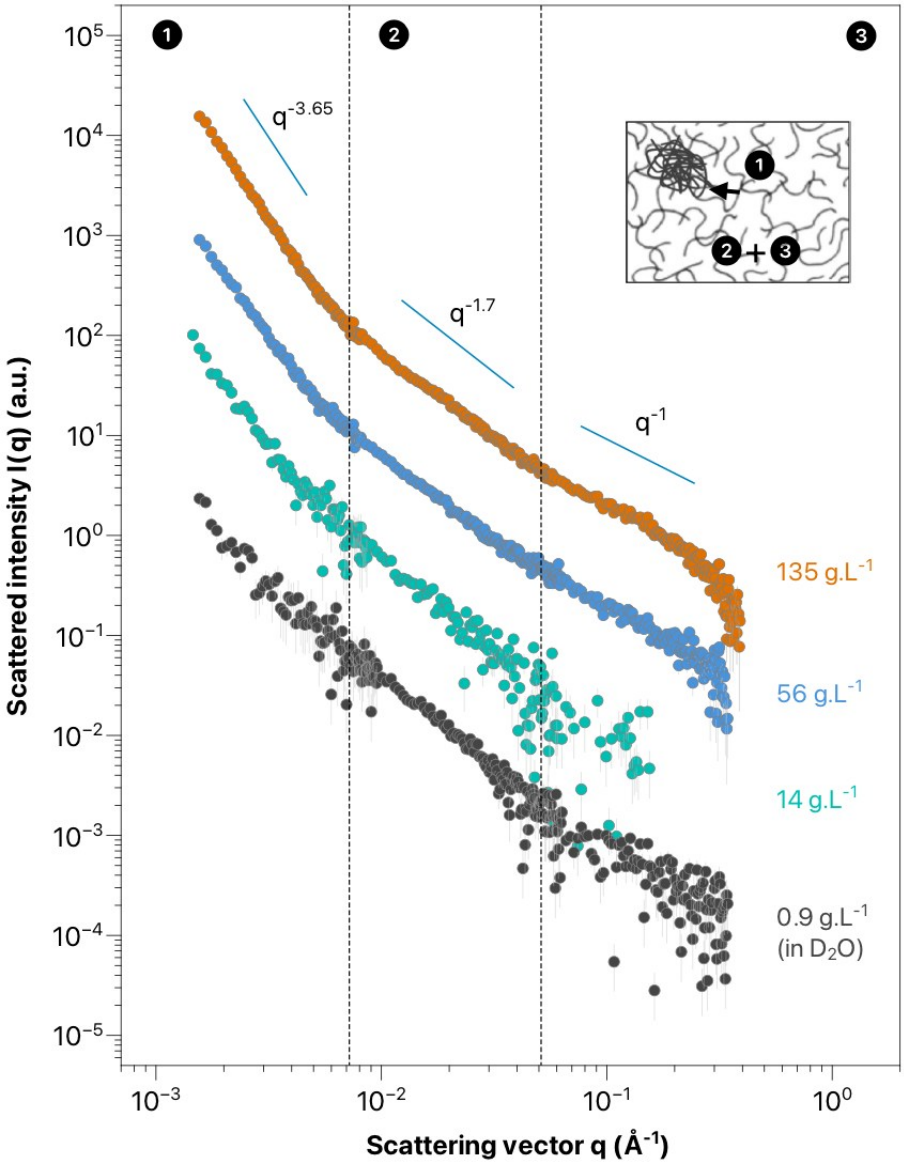

Figure 3. The SANS intensities of AX solutions from 0.9 to 135 g.L^{-1}. The data have been shifted along the *y*-axis for clarity. For all concentrations, the SANS profiles can be divided into three distinct *q*-regions where different length scales are explored (see the inset and the discussion below). In Supporting Information Figures S4 and S5, we give alternative representations of these results to better show the agreement between the proposed slopes in regions 2 and 3 and the data at the lowest concentrations (except for 14 g.L^{-1} in region 3 where the statistics is clearly not good enough to conclude).

For the naked eye, the general shape of the scattering curves appears quite similar at all concentrations (Figure 3). On all curves, we clearly identify three distinct q-regions, noted 1, 2, and 3, which correspond to structural information at different length scales, i.e., from large (few hundreds of nanometers) to local dimensions (Ångströms), respectively:

. **Region 1** ($q < 7.5\times10^{-3}$ Å^{-1}) shows a sharp rise in intensity towards low q-values which is the signature of the clusters that we discuss earlier. These clusters are also observed in XG solutions in pure water using static light scattering (SLS),[27] and using SANS in solutions of gel-forming AX extracted from *Plantago ovata* but in non-gelled, highly basic conditions.[18] We observe the same power-law behavior over the entire q-range of region 1, which indicates that the size of these objects is most likely $> 2\pi/q_{min} \approx 400$ nm. The slope of the signal, estimated from the data with the best statistics (135 g.L^{-1}), is about $q^{-3.65}$. This suggests that the clusters are rough 3D entities,[18] with a surface fractal dimension D_s given by $I_c(q) \sim q^{(6-D_s)}$, i.e., $D_s = 2.35$.[37] As discussed in the previous section, we can reasonably consider that the mass concentration of those objects is low compared to the concentration of the free AX chains in solution. Furthermore, the fact that the shape of the SANS profile does not change much with concentration suggests that the relative number of clusters (scattered intensity in region 1) does not change either with the total number of AX chains (intensity in regions 2 and 3). However, the analysis becomes speculative at this point as we do not know if the cluster size changes with AX concentration. Also, we will not go further into this discussion as the purpose of this work is to examine the characteristics of the free AX chains in solution, i.e., using the SANS information in regions 2 and 3.

. **Region 2** (7.5×10^{-3} Å$^{-1} < q < 5.5\text{x } 10^{-2}$ Å^{-1}) corresponds to the solution structure at intermediate scale, i.e., ~10-100 nm. On a log-log scale, the scattering curves all appear as quasi-linear in this region (Figure 3), with a power law $\sim q^{-1.7}$. This exponent value is characteristic of a polymer chain

in good solvent; meaning the AX chain adopts the conformation of a real, self-avoiding chain with excluded volume effects.[22,38,39] The 1.7 value corresponds to the theoretical Flory exponent ν = 1/1.7 = 0.588 for such a situation; where ν describes the relation between the size of a single, free polymer coil (R_g) and the number N of repetition units that compose the chain, i.e., $R_g \sim N^{\nu}$. To our knowledge, it is the first time that a Flory parameter of 0.588 -and the underlying self-avoiding statistic- is unambiguously determined for water-soluble AX. As discussed by Picout et al., it is indeed not possible to obtain a good approximation of that parameter using the former SEC-MALS results of Dervilly-Pinel on similar AX polymers.[20,21] On the other hand, the recent SANS results of Yu with AX from *Plantago ovata* seed mucilage also shows a $q^{-1.7}$ decay of the scattered intensity in a similar q-range.[18] But in this case the AX is non-soluble in water, and the solubilization of the chains is forced by using 0.7 M KOD as solvent. The raw material and the experimental conditions are thus very different from those of the present work, which makes a direct comparison impossible (at least there is no contradiction between the two results). Finally, the self-avoiding statistical behavior of water-soluble AX chains is strongly reminiscent of the SANS work of Muller et al., who find the exact same behavior for XG solubilized in water.[22] This resemblance is noteworthy, and is certainly due to similarities between the properties and chemical nature of the two hemicelluloses: XG being also a neutral and linear water-soluble polysaccharide, made of a glucose backbone decorated with xylose residues; a fraction of them being substituted with galactose, and in some cases the galactose being further substituted with fucose.

. **Region 3** ($q > 5.5\text{x } 10^{-2}$ Å^{-1}) contains structural information at small length scale, i.e., from ~10 nm to a few Å. It starts with a clear inflexion of the scattering profile from $\sim q^{-1.7}$ to a $\sim q^{-1}$ dependency (Figure 3). The q^{-1} scaling law is characteristic of a 3D object with a mass fractal D_m = 1, meaning the chain behaves as a rod at this length scale. This indicates that the AX polymer

can be pictured as a semiflexible chain, made of N connected rods/segments of a given length, the Kuhn length l_K.[39] The Kuhn length l_K, or perhaps the more commonly used persistence length $l_p = l_K/2$, gives a direct indication of the chain stiffness: a higher persistence length indicates a stiffer chain. In the SANS profiles, the persistence length is related to $I(q)$ at the transition from $\sim q^{-1.7}$ to $\sim q^{-1}$. In the next section, we determine precisely l_p by modeling the SANS data in this zone. At still higher q-values (from $q \approx 0.2$ Å^{-1}), the scattered intensity deviates from the q^{-1} power law, with a progressive and sharper decrease in I with q. This is the signature of thick rods, where the deviation from the q^{-1} exponent gives an indication on the radius of gyration of the cross section of the rods, R_c. Again, we show in the following section how to quantify precisely R_c using an adequate model.

SANS / Single chain. Here the objective is to quantify precisely the two parameters of the AX chain at the local scale which are its stiffness, i.e., the persistence length l_p, and its cross-section R_c. The approach consists in fitting the data to a model that considers these two parameters, plus the fact that the chain is in good solvent condition, i.e., with excluded volume effects. An analytical expression for such a worm-like chain (WLC) model has been proposed recently by Boze et al.,[40] based on the earlier work of Sharp and Bloomfeld.[41]

$$I_{\mathrm{WLC}}(q) = I_0 \left[\frac{2(e^{-x}+x-1)}{x^2} + \frac{2l_p}{L}\left[\frac{4}{15} + \frac{7}{15x} - \left(\frac{11}{15} + \frac{7}{15x}\right)e^{-x}\right]\right] exp\left(\frac{-q^2R_c^2}{2}\right) \quad (4)$$

where $x = q^2 \frac{Ll_p}{3}$, I_0 is the intensity scattered at $q \to 0$, L is the contour length of the chain (i.e., the length at maximal extension), l_p its persistence length, and R_c the polymer equivalent cross-section radius. This model is clearly equivalent to the one used by Muller et al. for XG chains,[22] and that is implemented in the SASfit software.[42]

For the fit, we use the SANS profile at 135 g.L^{-1} as it shows the best statistics at high q-values (more data points, small error bars). Also, it is safe to assume that the local chain dimensions l_p and R_c do not change with C and -more importantly- are contained in the SANS profile at 135 g.L^{-1} as it shows both the transition from a $q^{-1.7}$ to a q^{-1} power law and the further decrease in intensity that corresponds to the Guinier's law of the chain cross-section. Quite obviously, region 1 is not considered in the fit, as it corresponds to the associative clusters in the solution. In addition, we do not consider either the low q-values of region 2 (2×10^{-2} Å$^{-3} < q < 2\times10^{-2}$ Å^{-1}) in the fit, as the slope of the intensity decay is not strictly -1.7 in that case. This subtle but existing deviation from the 'average' slope of ~-1.7 (Figure 3) in this q-range is due to the fact that 135 g.L^{-1} is way over the overlap concentration $C^* \approx$ 3.3-3.9 g.L^{-1}. As a result, the correlation length information ξ is also contained in region 2 (see next section), thus creating the small deviation in the SANS signal at $q \approx 2\times10^{-2}$ Å^{-1} (Figure 4). Conversely, the WLC model strictly predicts a power law $\sim q^{-1.7}$ for a single chain at intermediate length scale, hence our choice to not use the data of region 2 at $q < 2\times10^{-2}$ Å^{-1} in the fit. Also, at $C > C^*$, the chains overlap, and the L parameter has no physical meaning in the WLC form factor model. L is then fixed to an arbitrary large value (1 μm), so that it does not intervene in the fit in the chosen q-region. The I_0 value, which depends on the L parameter, has no direct physical meaning either and is not discussed in the following.

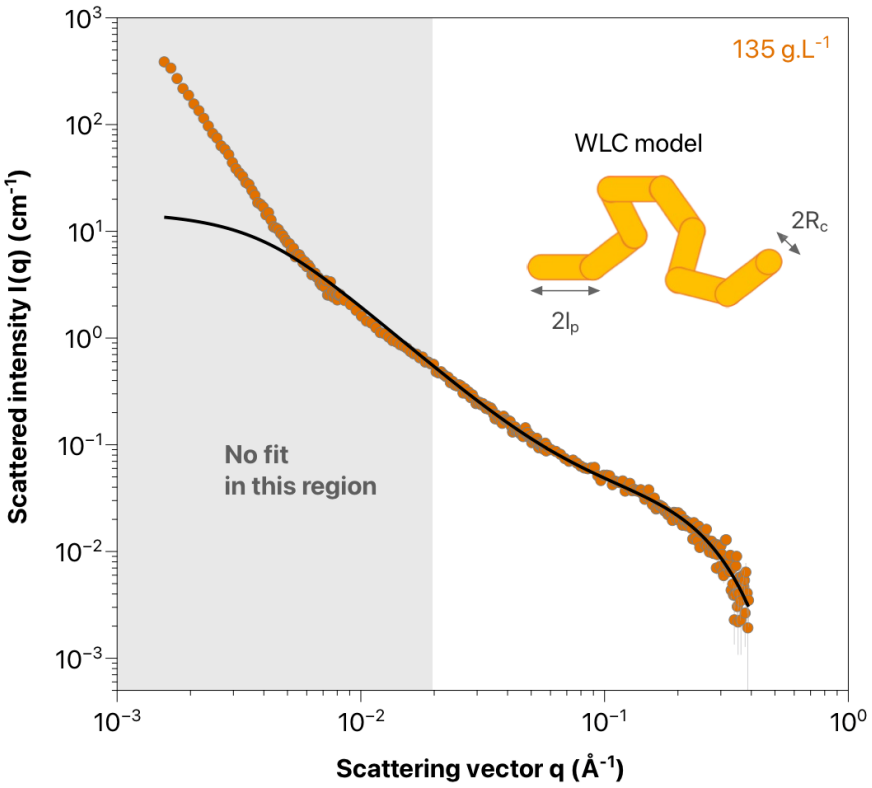

Figure 4. The fit of the experimental data at 135 g.L^{-1} AX (orange) to the WLC model described in the text (black line).

The fit consists in varying I_0, l_p and R_c to minimize the distance between the model and the experimental data at $q > 2\times10^{-2}$ Å^{-1}. The result is clearly excellent, as shown in Figure 4, with the best fit giving l_p = 45.0 Å and R_c = 5.8 Å. The value of the persistence length is characteristic of a semiflexible, relatively stiff polymer, as compared to much more flexible polymers like PEG for instance (l_p = 3.8 Å[43]). The obtained value contrasts with the 86 Å value estimated from SEC-MALS data obtained with a similar AX by Dervilly-Pinel et al.[20] However it is consistent with the 30 Å average value estimated by Picout et al. from the same SEC-MALS data but using calculations based on different theoretical considerations.[21] Clearly, the SANS technique gives a much more precise quantification of the AX persistence length. The value of 45.0 Å corresponds

to an elementary Kuhn segment of ~17 xylose units ($l_K = 2l_p$, Figure 5).[17] In comparison, the SANS-measured persistence length of water-soluble XG from tamarind seeds is about twice this size, i.e., 80 Å.[22] The reason for that is not straightforward but is probably a combination between the difference in chemical nature of the backbone (glucose vs. xylose), and the fact that XG has a different substitution pattern than AX, with more side chain residues and in some cases galactose substitutions on the decorating xyloses.[22] The comparison is probably more direct with the SAXS experiments performed by Yu et al. with AX from *Plantago ovata* seed.[18] In that case, the measured persistence length of AX solubilized in 0.7 M KOD solution is 45-47 Å, which is very similar to our result. Regarding the cross-section of the equivalent polymer segment, the value that we obtain, i.e., $2R_c$ = 11.6 Å, is about twice the average size of one xylose or arabinose residue (5-6 Å),[17] which is fully consistent with the AX chain structure and composition (Figure 5). Interestingly, the cross-sections reported by Yu et al. for the *Plantago ovata* AX polymer are much larger, with $2R_c \approx$ 18-22 Å. It is probably because this peculiar, gel-forming, AX (i) has presumably a higher number of arabinose side-chain residues than the AX used in the present study,[18] (ii) has a less linear backbone structure that contains some atypical β-1,3 linked xylose residues.[44]

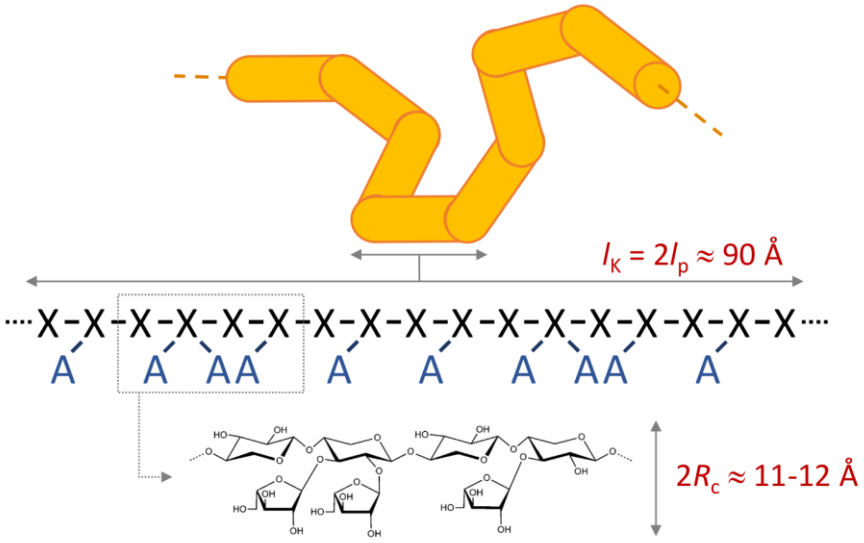

Figure 5. A schematic representation of the WLC structure of the water-soluble AX used in the present study, together with the local parameter l_p and R_c obtained from the model.

SANS / Semidilute solutions. In the semidilute regime, i.e., when the AX concentration exceeds C^*, the polymer chains get closer together and start to overlap. When this happens, a characteristic distance emerges which is the correlation length ξ of the polymer solution. ξ is the average distance from one monomer of one chain to the nearest monomer of another chain.[25,45] It is a parameter of fundamental importance, as it controls -for instance- the diffusivity of particles in the polymer solution. In a common polymer solution, ξ is directly linked to the q-value at which a plateau appears in the SAXS or SANS intensity at low q.[38,46] In our case, the analysis is complicated by the presence of large objects in this q-range, which literally hides such a plateau behavior at low and intermediate length scale (regions 1 and 2). To leverage this difficulty, we fit our data to a simple model that considers the scattered intensity as resulting from two independent contributions:

. $I_c(q)$, the contribution of the associative clusters at low q. We do not know their size neither their internal organization, but they have a surface fractal dimension $D_s \approx 2.35$, so that, in the explored q-range,

$$I_c(q) = A\, q^{-(6-D_s)} = \text{A}\, q^{-3.65} \quad (5)$$

with A a scaling factor

. $I_s(q)$, the contribution of the AX solution of correlation length ξ. Following the work of Falcao et al., we do not use the standard Ornstein-Zernike function (also called Lorentzian scattering law) for $I_s(q)$, as this expression is only valid in a small q-range, i.e., until the scattered intensity starts to decrease at $q \approx 1/\xi$.[46] Instead, we use the expression of these authors, which was built specifically for fitting the data over a larger q-range, including the q-values where the intensity decays as $q^{-1.7}$ (end of region 2)[46]

$$I_s(q) = B\, \frac{(1+q\xi)^{1/3}}{1+q^2\xi^2} \quad (6)$$

with B a second scaling factor

The total intensity is then obtained by adding up the two contributions

$$I_s(q) = I_c(q) + I_s(q) \quad (7)$$

And the only adjustable parameters of the model are A, B and ξ.

Note that this basic model does not describe the semidilute solution at small scale, i.e., where the SANS profile is related to the local properties of the chain (l_p and R_c, see previous section). Therefore, we exclude this length scale from the fitting procedure and only use the experimental data obtained at $q > 5 \times 10^{-2}$ Å^{-1}. The results of the fits are given in Figures 6-8.

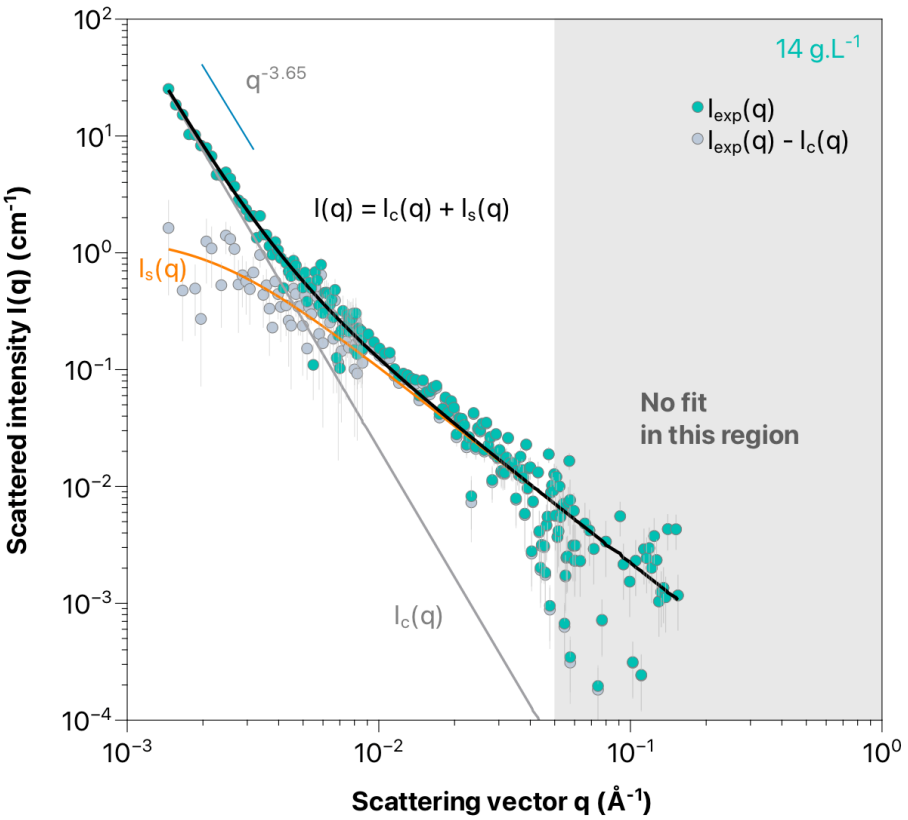

Figure 6. The SANS profile of the 14 g.L^{-1} AX sample (green circles, $I_{exp}(q)$), with the fit of the experimental data to the composite model described in the text (black line, $I(q)$). The gray line, $I_c(q)$, is the contribution of the clusters to the scattered intensity calculated from the model, while the orange line, $I_s(q)$, is the contribution of the dissolved AX chains. The light gray circles are the experimental intensities after subtraction of the cluster contribution $I_c(q)$ obtained from the fit of the model.

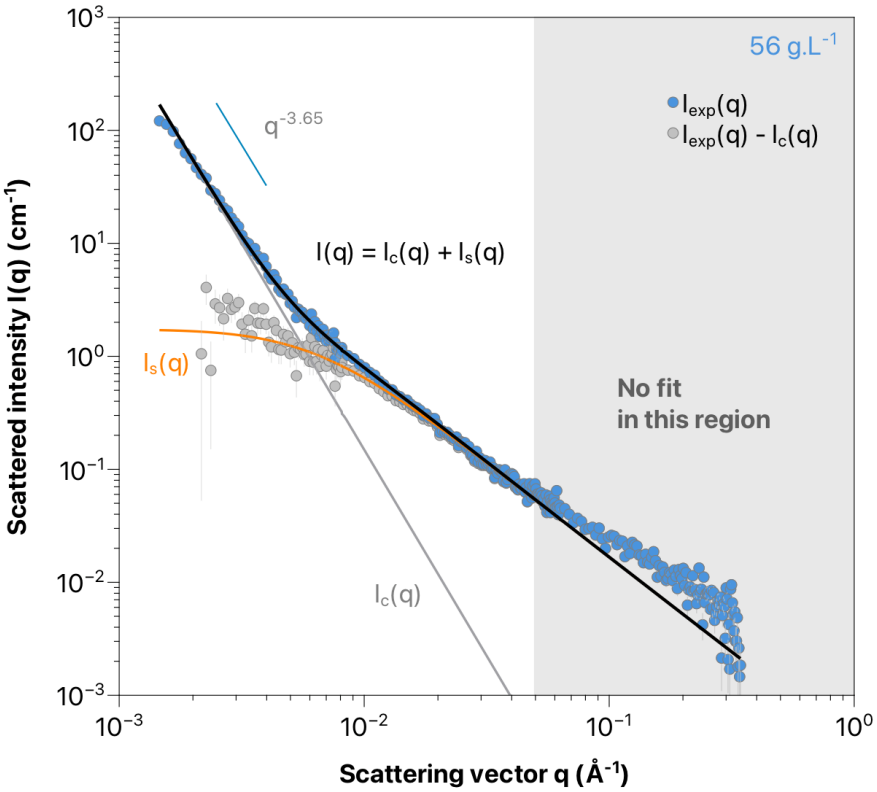

Figure 7. The SANS profile of the 56 g.L^{-1} AX sample (blue circles, $I_{exp}(q)$), with the fit of the experimental data to the model described in the text (black line, $I(q)$).

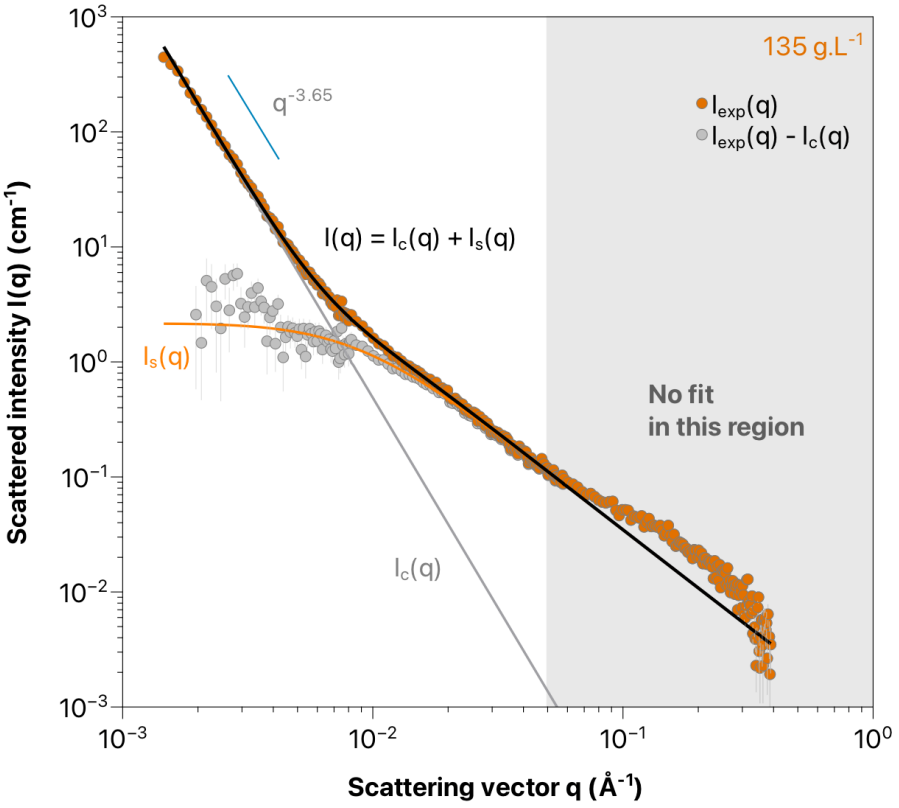

Figure 8. The SANS profile of the 135 g.L^{-1} AX sample (orange circles, $I_{exp}(q)$), with the fit of the experimental data to the model described in the text (black line, $I(q)$).

The fits (black lines) are very satisfactory for all the concentrations investigated. For clarity, Figures 6-8 also give the two individual contributions $I_c(q)$ and $I_s(q)$ to the total scattering, as given by eqs 5 and 6. $I_s(q)$ has this characteristic shape with a tendency towards a plateau value at low q and the transition to a progressive decay in $q^{-1.7}$ when the explored length scale approaches the correlation length ξ. Knowing the contribution of the clusters $I_c(q)$, it is also possible to calculate the difference $I_{exp}(q)$-$I_c(q)$ between the experimentally measured scattered intensities and the cluster contribution as obtained from the fit (gray circles). In all cases, and especially when the statistics is good (135 and 56 g.L^{-1}), we see that the obtained data nicely align with the theoretical polymer intensities within the inflexion zone, i.e., from 4×10^{-3} – 2×10^{-2} Å^{-1}. This suggests that

our modelling approach, despite its relative simplicity, is quite consistent. Note that the correspondence between I_{exp}(q)-$I_c(q)$ and $I_s(q)$ is less marked at lower q-values. This is because the contribution of the clusters is dominant in this region, leading to less reliable values for I_{exp}(q)-$I_c(q)$.

Figure 9 gives the correlation lengths ξ obtained from the fits at concentrations 14, 56 and 135 g.L^{-1}. In addition, we give the ξ value obtained from a fit to the SANS data measured in D_2O at 0.9 g.L^{-1} (see Figure S6). By definition, ξ is the length beyond which interchain correlations overtake intrachain correlations. When C < C*, as it is the case at 0.9 g.L^{-1}, interchain correlations are negligible. Therefore ξ should corresponds to the space occupied by one single chain in solution, meaning $\xi \approx R_g$. The R_g value obtained by SEC-MALS at 1 g.L^{-1} is reported in Figure 9. As expected, ξ and R_g are indeed very close. As C then increases and exceeds C*, the chains progressively overlap and interchain correlations gradually overtake intrachain correlations. This results in the decrease of the correlation length ξ with C. As shown experimentally with several polymer systems,[46,47] the crossover from dilute to semidilute solutions can occur over about one decade in concentration, which appears to be the case for our system as well (~2-20 g.L^{-1}). At further higher concentrations, interchain correlations must dominate so that the correlation length ξ should decrease according to the scaling theory for semidilute polymer solution in good solvent, i.e., $\xi \sim C^{-\nu/(3\nu-1)} = C^{-0.77}$.[25,38] Figure 9 gives the comparison between our data and the theory, showing a very good agreement between the two. Clearly, this result further confirms that the AX chains can be considered as polymer chains in good solvent, as already stated from the general shape of the SANS profiles at intermediate length scale (Figures 3 and 4).

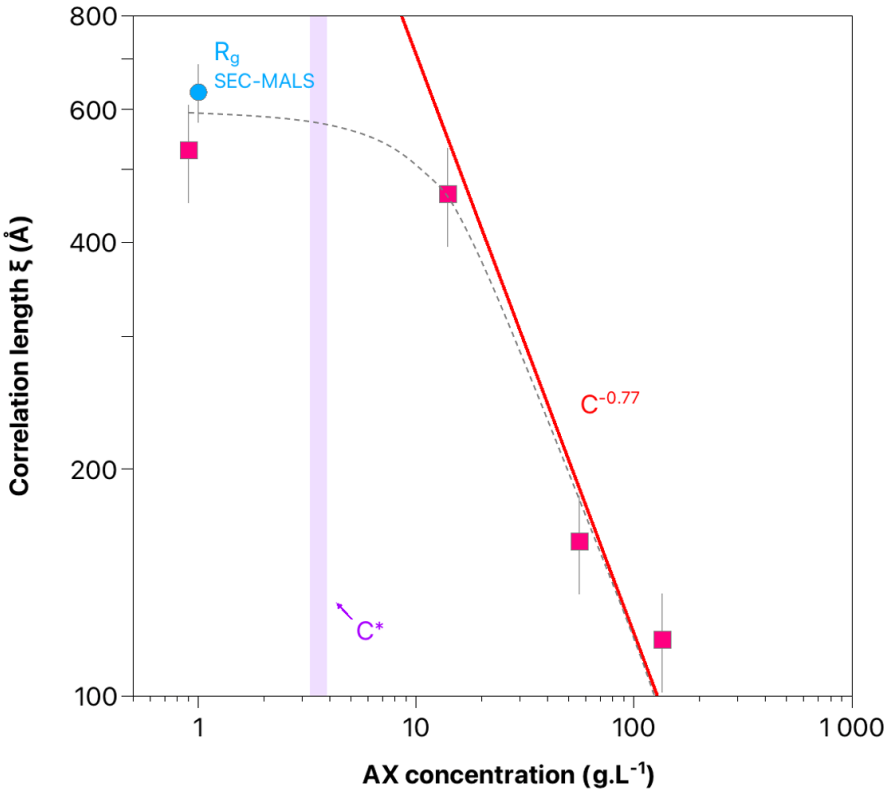

Figure 9. Crossover from dilute to semidilute solutions of AX.Variation of the correlation length ξ obtained from the fits of our model as a function of AX concentration. The straight line gives the $C^{-0.77}$ dependence that is expected for semidilute solutions of polymer chains in good solvent.[25,46] The vertical thick line corresponds to the C^* values obtained from rheology. For comparison, we give the R_g value obtained from SEC-MALS at 1 g.L^{-1} AX. The dashed line is a guide for the eye.

CONCLUSIONS

Using SANS, complemented with SEC-MALS and viscosity measurements, we were able to obtain a complete characterization of the structure and conformational behavior of a generic arabinoxylan (AX, extracted from wheat-flour) when dispersed in a sodium phosphate aqueous buffer solution. Our first finding, that is consistent with observations made with another major hemicellulose (xyloglucan XG),[22,27] is the fact that despite the large solubility of AX in water, it

is not possible to fully get rid of the associative interactions between some AX chains. This results in the presence of some large objects (> 500 nm), that we call clusters in the present study, but at a concentration that is too small for having an effect on the viscosity of the AX solutions. In a second step, we examine closely the SANS profile of AX solutions in the intermediate and high q-ranges. This allows us to unambiguously determine that the AX chains behave as a polymer in good solvent, adopting the statistical conformation of a self-avoiding chain with excluded effects. A worm-like chain model fits the data nicely at these length scales, allowing us to quantify accurately the stiffness of the polymer, l_p = 45 Å, and its average cross-section size, $2R_c$ = 11-12 Å. Finally, we focus on the SANS data at low and intermediate q-ranges, with the aim of understanding how the chains behave when entering the semidilute concentration regime, i.e., $C > C^*$. For that, we follow a simple modeling approach that allows us to extract the correlation length ξ of the polymer solution from the SANS profiles, in conditions spanning more than two decades of concentrations (~1-135 g.L^{-1}). The change in ξ as the macromolecules get closer together with concentration is fully consistent with the behavior of a polymer in good solvent, especially in the high concentration regime where the data closely follow the scaling theory that is expected in that case.

We believe that such a thorough and unprecedented characterization of AX in a sodium phosphate pH-buffered aqueous solution, from low to high concentrations, provides a variety of information that are both of fundamental and practical interests: (i) fundamental as our work gives a unique complement to the -still scarce- SAXS and SANS studies dedicated to the conformational behavior of hemicellulosic polymers in solution,[18,22] (ii) practical as AX can potentially be used as a substitute to oil-based molecules in many applications that our results may contribute to develop and/or control.

ASSOCIATED CONTENT

Supporting Information.

The Supporting Information is available free of charge on the ACS publication website at DOI: SAXS preliminary experiments for the determination of the best solubilization process, determination of the increment of refractive index for arabinoxylan, SEC-MALS results, fit of the correlation length ξ model to the SANS data obtained at 0.9 g/L (PDF)

AUTHOR INFORMATION

Corresponding Author

*E-mail antoine.bouchoux@insa-toulouse.fr

Author Contributions

All authors have given approval to the final version of the manuscript. MP and LD contributed equally to the work.

Notes

The authors declare no competing financial interest

ACKNOWLEDGMENTS

We thank Pascale Laborie for her technical assistance on the SEC-MALS experiments (Technopolym analysis platform, Université de Toulouse, CNRS, Toulouse), as well as the research federation FERMaT (Université de Toulouse, CNRS, INSA Toulouse, Toulouse INP) for providing access to the SAXS instrument. We also thank L. Ramos from Laboratoire Charles Coulomb (Université de Montpellier, CNRS, Montpellier) for fruitful discussions.

ABBREVIATIONS

AX, arabinoxylan; A, arabinose; X, xylose; SEC, size exclusion chromatography; MALS, multi-angle laser light scattering; SAXS, small angle X-ray scattering; SANS, small angle neutron scattering; XG, xyloglucan; NMR, nuclear magnetic resonance; HPLC, high performance liquid chromatography; RI, refractive index; light scattering, LS

REFERENCES

(1) Sarkar, P.; Bosneaga, E.; Auer, M. Plant Cell Walls throughout Evolution: Towards a Molecular Understanding of Their Design Principles. *J. Exp. Bot.* **2009**, *60* (13), 3615–3635.

(2) Gao, S.; Song, W.; Guo, M. The Integral Role of Bioproducts in the Growing Bioeconomy. *Ind. Biotechnol.* **2020**, *16* (1), 13–25.

(3) Smith, P. J.; Wang, H.-T.; York, W. S.; Peña, M. J.; Urbanowicz, B. R. Designer Biomass for Next-Generation Biorefineries: Leveraging Recent Insights into Xylan Structure and Biosynthesis. *Biotechnol. Biofuels Bioprod.* **2017**, *10* (1), 286.

(4) Grantham, N. J.; Wurman-Rodrich, J.; Terrett, O. M.; Lyczakowski, J. J.; Stott, K.; Iuga, D.; Simmons, T. J.; Durand-Tardif, M.; Brown, S. P.; Dupree, R.; Busse-Wicher, M.; Dupree, P. An Even Pattern of Xylan Substitution Is Critical for Interaction with Cellulose in Plant Cell Walls. *Nat. Plants* **2017**, *3* (11), 859–865.

(5) de O. Buanafina, M. M. Feruloylation in Grasses: Current and Future Perspectives. *Mol. Plant* **2009**, *2* (5), 861–872.

(6) Izydorczyk, M. S.; Biliaderis, C. G. Cereal Arabinoxylans: Advances in Structure and Physicochemical Properties. *Carbohydr. Polym.* **1995**, *28* (1), 33–48.

(7) Yan, J.; Jia, X.; Feng, L.; Yadav, M.; Li, X.; Yin, L. Rheological and Emulsifying Properties of Arabinoxylans from Various Cereal Brans. *J. Cereal Sci.* **2019**, *90*, 102844.

(8) Chen, Z.; Li, S.; Fu, Y.; Li, C.; Chen, D.; Chen, H. Arabinoxylan Structural Characteristics, Interaction with Gut Microbiota and Potential Health Functions. *J. Funct. Foods* **2019**, *54*, 536–551.

(9) Höije, A.; Sternemalm, E.; Heikkinen, S.; Tenkanen, M.; Gatenholm, P. Material Properties of Films from Enzymatically Tailored Arabinoxylans. *Biomacromolecules* **2008**, *9* (7), 2042–2047.

(10) Carvajal-Millan, E.; Landillon, V.; Morel, M.-H.; Rouau, X.; Doublier, J.-L.; Micard, V. Arabinoxylan Gels: Impact of the Feruloylation Degree on Their Structure and Properties. *Biomacromolecules* **2005**, *6* (1), 309–317.

(11) Mikkelsen, D.; Flanagan, B. M.; Wilson, S. M.; Bacic, A.; Gidley, M. J. Interactions of Arabinoxylan and (1,3)(1,4)-β-Glucan with Cellulose Networks. *Biomacromolecules* **2015**, *16* (4), 1232–1239.

(12) Köhnke, T.; Östlund, Å.; Brelid, H. Adsorption of Arabinoxylan on Cellulosic Surfaces: Influence of Degree of Substitution and Substitution Pattern on Adsorption Characteristics. *Biomacromolecules* **2011**, *12* (7), 2633–2641.

(13) Köhnke, T.; Lin, A.; Elder, T.; Theliander, H.; Ragauskas, A. J. Nanoreinforced Xylan–Cellulose Composite Foams by Freeze-Casting. *Green Chem.* **2012**, *14* (7), 1864–1869.

(14) Talantikite, M.; Beury, N.; Moreau, C.; Cathala, B. Arabinoxylan/Cellulose Nanocrystal Hydrogels with Tunable Mechanical Properties. *Langmuir* **2019**, *35* (41), 13427–13434.

(15) Warrand, J.; Michaud, P.; Picton, L.; Muller, G.; Courtois, B.; Ralainirina, R.; Courtois, J. Contributions of Intermolecular Interactions between Constitutive Arabinoxylans to the Flaxseeds Mucilage Properties. *Biomacromolecules* **2005**, *6* (4), 1871–1876.

(16) Dervilly, G. Isolation and Characterization of High Molar Mass Water-Soluble Arabinoxylans from Barley and Barley Malt. *Carbohydr. Polym.* **2002**, *47* (2), 143–149.

(17) Dervilly, G.; Saulnier, L.; Roger, P.; Thibault, J.-F. Isolation of Homogeneous Fractions from Wheat Water-Soluble Arabinoxylans. Influence of the Structure on Their Macromolecular Characteristics. *J. Agric. Food Chem.* **2000**, *48* (2), 270–278.

(18) Yu, L.; Yakubov, G. E.; Martínez-Sanz, M.; Gilbert, E. P.; Stokes, J. R. Rheological and Structural Properties of Complex Arabinoxylans from Plantago Ovata Seed Mucilage under Non-Gelled Conditions. *Carbohydr. Polym.* **2018**, *193*, 179–188.

(19) Andrewartha, K. A.; Phillips, D. R.; Stone, B. A. Solution Properties of Wheat-Flour Arabinoxylans and Enzymically Modified Arabinoxylans. *Carbohydr. Res.* **1979**, *77* (1), 191–204.

(20) Dervilly-Pinel, G.; Thibault, J.-F.; Saulnier, L. Experimental Evidence for a Semi-Flexible Conformation for Arabinoxylans. *Carbohydr. Res.* **2001**, *330* (3), 365–372.

(21) Picout, D. R.; Ross-Murphy, S. B. On the Chain Flexibility of Arabinoxylans and Other β-(1→4) Polysaccharides. *Carbohydr. Res.* **2002**, *337* (19), 1781–1784.

(22) Muller, F.; Manet, S.; Jean, B.; Chambat, G.; Boué, F.; Heux, L.; Cousin, F. SANS Measurements of Semiflexible Xyloglucan Polysaccharide Chains in Water Reveal Their Self-Avoiding Statistics. *Biomacromolecules* **2011**, *12* (9), 3330–3336.

(23) Tao, H.; Huang, C.; Lodge, T. P. Correlation Length and Entanglement Spacing in Concentrated Hydrogenated Polybutadiene Solutions. *Macromolecules* **1999**, *32* (4), 1212–1217.

(24) Lopez, C. G.; Horkay, F.; Mussel, M.; Jones, R. L.; Richtering, W. Screening Lengths and Osmotic Compressibility of Flexible Polyelectrolytes in Excess Salt Solutions. *Soft Matter* **2020**, *16* (31), 7289–7298.

(25) Cai, L.-H.; Panyukov, S.; Rubinstein, M. Mobility of Nonsticky Nanoparticles in Polymer Liquids. *Macromolecules* **2011**, *44* (19), 7853–7863.

(26) McCleary, B. V.; McKie, V. A.; Draga, A.; Rooney, E.; Mangan, D.; Larkin, J. Hydrolysis of Wheat Flour Arabinoxylan, Acid-Debranched Wheat Flour Arabinoxylan and Arabino-Xylo-Oligosaccharides by β-Xylanase, α-l-Arabinofuranosidase and β-Xylosidase. *Carbohydr. Res.* **2015**, *407*, 79–96.

(27) Muller, F.; Jean, B.; Perrin, P.; Heux, L.; Boué, F.; Cousin, F. Mechanism of Associations of Neutral Semiflexible Biopolymers in Water: The Xyloglucan Case Reveals Inherent Links. *Macromol. Chem. Phys.* **2013**, *214* (20), 2312–2323.

(28) Bonnet-Gonnet, C.; Belloni, L.; Cabane, B. Osmotic Pressure of Latex Dispersions. *Langmuir* **1994**, *10* (11), 4012–4021.

(29) Parsegian, V. A.; Rand, R. P.; Fuller, N. L.; Rau, D. C. Osmotic Stress for the Direct Measurement of Intermolecular Forces. In *Methods Enzymol.*; Biomembranes Part O: Protons and Water: Structure and Translocation; Academic Press, 1986; Vol. 127, pp 400–416.

(30) Cohen, J. A.; Podgornik, R.; Hansen, P. L.; Parsegian, V. A. A Phenomenological One-Parameter Equation of State for Osmotic Pressures of PEG and Other Neutral Flexible Polymers in Good Solvents. *J. Phys. Chem. B* **2009**, *113* (12), 3709–3714.

(31) Pasquier, C.; Beaufils, S.; Bouchoux, A.; Rigault, S.; Cabane, B.; Lund, M.; Lechevalier, V.; Le Floch-Fouéré, C.; Pasco, M.; Pabœuf, G.; Pérez, J.; Pezennec, S. Osmotic Pressures of Lysozyme Solutions from Gas-like to Crystal States. *Phys. Chem. Chem. Phys.* **2016**, *18* (41), 28458–28465.

(32) Bouchoux, A.; Cayemitte, P. E.; Jardin, J.; Gésan-Guiziou, G.; Cabane, B. Casein Micelle Dispersions under Osmotic Stress. *Biophys. J.* **2009**, *96* (2), 693–706.

(33) Jacrot, B.; Zaccai, G. Determination of Molecular Weight by Neutron Scattering. *Biopolymers* **1981**, *20*, 2413–2426.

(34) Yeh, Y.-L. Real-Time Measurement of Glucose Concentration and Average Refractive Index Using a Laser Interferometer. *Opt.Lasers Eng.* **2008**, *46* (9), 666–670.

(35) Cheng, Y.; Brown, K. M.; Prud'homme, R. K. Characterization and Intermolecular Interactions of Hydroxypropyl Guar Solutions. *Biomacromolecules* **2002**, *3* (3), 456–461.

(36) Krause, W. E.; Bellomo, E. G.; Colby, R. H. Rheology of Sodium Hyaluronate under Physiological Conditions. *Biomacromolecules* **2001**, *2* (1), 65–69.

(37) Wei, Y; Hore, M. J. A., Characterizing polymer structure with small-angle neutron scattering: A Tutorial. *J. Appl. Phys.*, **2021**, 129, 171101.

(38) de Gennes, P.-G. *Scaling Concepts in Polymer Physics*; Cornell University Press, 1979.

(39) Teraoka, T. *Polymer Solutions: An Introduction to Physical Properties*; Wiley, 2002.

(40) Boze, H.; Marlin, T.; Durand, D.; Pérez, J.; Vernhet, A.; Canon, F.; Sarni-Manchado, P.; Cheynier, V.; Cabane, B. Proline-Rich Salivary Proteins Have Extended Conformations. *Biophys. J.* **2010**, *99* (2), 656–665.

(41) Sharp, P.; Bloomfield, V. A. Light Scattering from Wormlike Chains with Excluded Volume Effects. *Biopolymers* **1968**, *6* (8), 1201–1211.

(42) Breßler, I.; Kohlbrecher, J.; Thünemann, A. F. SASfit: A Tool for Small-Angle Scattering Data Analysis Using a Library of Analytical Expressions. *J. Appl. Crystallogr.* **2015**, *48* (5), 1587–1598.

(43) Lee, H.; Venable, R. M.; MacKerell, A. D.; Pastor, R. W. Molecular Dynamics Studies of Polyethylene Oxide and Polyethylene Glycol: Hydrodynamic Radius and Shape Anisotropy. *Biophys. J.* **2008**, *95* (4), 1590–1599.

(44) Yu, L.; Yakubov, G. E.; Zeng, W.; Xing, X.; Stenson, J.; Bulone, V.; Stokes, J. R. Multi-Layer Mucilage of Plantago Ovata Seeds: Rheological Differences Arise from Variations in Arabinoxylan Side Chains. *Carbohydr. Polym.* **2017**, *165*, 132–141.

(45) Sorichetti, V.; Hugouvieux, V.; Kob, W. Determining the Mesh Size of Polymer Solutions via the Pore Size Distribution. *Macromolecules* **2020**, *53* (7), 2568–2581.

(46) Falcao, A. N.; Pedersen, J. S.; Mortensen, K. Structure of Randomly Crosslinked Poly(Dimethylsiloxane) Networks Produced by Electron Irradiation. *Macromolecules* **1993**, *26* (20), 5350–5364.

(47) Li, J.; Turesson, M.; Haglund, C. A.; Cabane, B.; Skepö, M. Equation of State of PEG/PEO in Good Solvent. Comparison between a One-Parameter EOS and Experiments. *Polymer* **2015**, *80*, 205–213.